Mohammad Y. Al-Haik*, Abdulmohsen A. Alothman and Muhammad R. Hajj

Integrated Thermoelectric Energy Generator and Organic Storage Device

https://doi.org/10.1515/ehs-2018-0009

Abstract: We evaluate the storage performance of an integrated energy harvesting and storage system using a thermoelectric generator (TEG) and an organic energy storage device. The power generated by the TEG is obtained by varying the temperature of the heat source on the bottom surface of the TEG while keeping the opposite surface at a constant cooling temperature. The difference in temperature gradient (ΔT) increases the power generated by the TEG. Capacitance-voltage measurements were performed on the organic storage device to evaluate the storage capabilities of the embedded storage elements, CdS nanoparticles. The objective is to assess the possibility of the integrated system and evaluate the effectiveness of the storage device. Voltage, current and power density values are determined and compared for different load resistance. The results revealed that for the 100 Ω load resistor, the voltage across the capacitor was the maximum at a lower temperature gradient with a charge density of $5.14 \times 10^{-3} \frac{C}{m^2}$.

Keywords: thermoelectric generator, organic capacitors, nanoparticles storage elements, integrated system, organic semiconductors

1 Introduction

A thermoelectric generator converts thermal energy into electrical energy and has the potential to be used in many applications that include energy recovery from waste heat to power sensors or charge storage devices such as batteries and capacitors. TEG can improve the efficiency of energy conversion systems by converting waste heat into electrical power (Ismail and Ahmed 2009). Recent efforts to predict power generated from thermoelectric generators using mathematical models have been proposed. Kristiansen et al. (2012) developed a mathematical model for various TEG models to predict the power harvested from marine incinerators that burn liquid and solid waste. A seawater heat sink was used to maintain the temperature difference required to generate sufficient power from the TEG. By implementing their model, the authors were able to validate the results and revealed a reduction in the cost per Watt for their particular TEG models. Samson et al. (2012) installed a TEG on an aircraft and tested it during flights. Based on the flight test, their proposed TEG showed high reliability for harvesting energy. Simliarly, thermoelectric generators have also been suggested for waste heat recovery from automobiles. Hsiao, Chang, and Chen (2010) investigated heat recovery of an internal combustion engine using thermoelectric generators, where the exhaust pipe and radiator are used as sources of heat. By placing the TEG on the exhaust pipe, the suggested optimum location, the maximum power harvested was 0.43 W for a temperature difference of 290 K. Hsu et al. (2011) investigated the power gained from automobile exhaust using 24 TEG modules. To increase the temperature gradient, the cold side of each module was attached to a heat sink and a fan. The maximum power harvested was 12.41 W at a temperature difference of 30 K while the engine was operational at 3500 RPM.

Thermoelectric generators, when provided with enough temperature difference, can generate very high levels of voltage and current, thus providing high levels of power. The excess levels of energy can be stored in a storage device for later use. Conventional storage devices, specifically capacitors, are a great choice for storing the energy generated. However, they can be harmful to the environment if not properly disposed of. Therefore, we suggest implementing an organic storage device with a TEG module. Organic storage devices can be a good replacement due to their low cost, high speed and simple fabrication process. The organic storage devices have a comparable structure setup to metal-insulator-semiconductor (MIS) devices which contain charging elements, insulating materials and organic

***Corresponding author: Mohammad Y. Al-Haik,** Department of Electromechanical Engineering Technology, Abu Dhabi Polytechnic, Abu Dhabi, UAE, 111499, E-mail: mohammad.alhaik@adpoly.ac.ae
Abdulmohsen A. Alothman, King Abdulaziz City for Science and Technology, National Satellite Technology Center, Riyadh, Saudi Arabia, E-mail: dr.alothman2@gmail.com
Muhammad R. Hajj, Department of Biomedical Engineering and Mechanics, Virginia Tech, Blacksburg, VA, USA, E-mail: mhajj@vt.edu

semiconductors all sandwiched between two conductive electrodes.

Sargentis et al. (2007); Mabrook et al. (2009, 2008) and Guan et al. (2007) showed that gold nanoparticles can be used as charging elements in fabricating MIS structured storage devices. All the above investigators were able to obtain comparative capacitance-voltage hysteresis window gates that showed gold nanoparticles are responsible for storing the generated charge. Other researchers also used different nanoparticles such as copper (Gupta et al. 2012), carbon nanotubes (Sleiman et al. 2012) and germanium (Duguay et al. 2007) in constructing storage devices. Furthermore, all the above mentioned researchers used silicon wafers as semiconductors. Haik et al. (2014) developed an organic storage device which used organic polymers as semiconductor and Au-Pt-Ag nanoparticles as charge storage elements. Their results showed large capacitance-voltage hysteresis loops that indicated storage within the nanoparticles when compared with a reference device that did not contain nanoparticles. The authors also revealed larger window gates when the organic polymers were used as the semiconductor to replace the silicon wafer.

In this effort, we construct a storage device that uses CdS as the storage elements and integrate it with a TEG module and evaluate the operating efficiency and storage capacity under various load resistance. We assess the voltage, current and power density levels produced from the TEG and evaluate the performance of the storage devices under the different operating conditions. The integration covers several conditions including steady and unsteady temperature gradients.

2 Organic Storage Device Fabrication

2.1 Material Preparation

The process of producing the organic polymer blend is discussed by Haik et al. (2014). Briefly, two non-conductive polymers were blended with an ionic liquid, glycerol, that acts as a plasticizer. The results showed that increasing the concentration levels increases the polymers conductivity. It was reported that 2 wt% of the plasticizer revealed great electrical conductivity values and is used amongst the other concentration percentages. Cadmium sulfide (CdS) nanoparticles were synthesized by chemical co-precipitation technique. The procedures of synthesizing the nanoparticles consisted of the following steps. First, 100 mL of 1 mM of cadmium chloride ($CdCl_2$) was added to 100 mL of sodium citrate dihydrate and magnetically stirred for 10 minutes. To this solution, 100 mL of sodium sulfide nonahydrate was added and stirred for 15 minutes. The yellow precipitate obtained is washed three times with deionized water and dried at 60^oC. The insulating material, poly methyl-methacrylate (PMMA), solution was produced by mixing 8 mg of PMMA powder in 1 mL of chloroform and left to mix overnight.

2.2 Organic Capacitor Fabrication

Figure 1 shows a schematic of the layer-by-layer setup of the organic storage device. Previous work showed that this layer-by-layer setup reveals larger storage capabilities. Therefore, the proposed setup will be discussed.

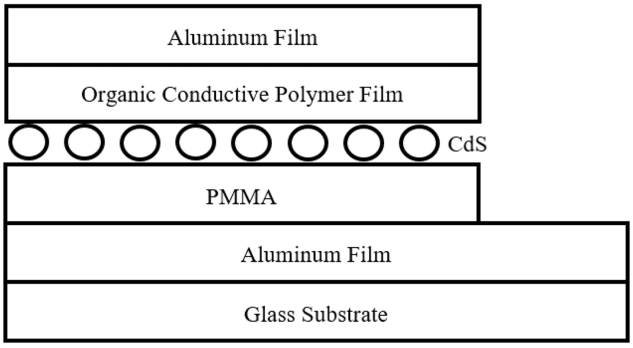

Figure 1: The layer-by-layer schematic of the device.

The organic capacitor consists of five layers. The bottom aluminum electrode layer was thermally evaporated on a glass substrate with a thickness of 100 nm. The glass substrate of dimensions 2 cm × 2 cm was used for handling purposes. After thermally evaporating the bottom electrode, the organic insulator, poly (methyl methacrylate) PMMA, was spin coated at 500 rmp for 10 seconds and then 5000 rpm for 50 s. This ensured uniform distribution of the insulating material. Then, the CdS storage elements were deposited on top of the PMMA layer by spin coating for one minute at the same rate. The organic semiconduting polymer was later spun coated over the storage elements. After each coating process, the sample was heated over a hot plate set at 50^oC to allow excess moisture to evaporate. Finally, the top aluminum electrode was thermally evaporated to a thickness of 100 nm.

Capacitance-voltage (C-V) sweeps of the organic storage device were performed using a Keithley 4200 semiconductor characterization system (SCS) computer

controlled analyzer to investigate the charge storage capability retained in the nanoparticles. The measurements were performed with a dual voltage sweep in the range of −20 V to +20 V and back to −20 V at a scan rate of 0.5 V/s. This was done to show the ability of the nanoparticles to act as charging elements by observing the presence of a hysteresis loop and the width of the window gap as a function of the voltage sweep range. The C-V measurement revealed the conventional accumulation (capacitor is charged) and inversion (capacitor is discharged) characteristics of a typical MIS device (Mabrook et al. 2009). The C-V measurements plot is reported in previous work (Al-Haik, Haik, and Hajj 2017).

The wide window gap observed in the hysteresis plots is a clear indication of the charge storage capability within the nanoparticles. This large hysteresis window is mainly linked to the high charge transport mobility of the carriers. Because a reference device with no particles (Al-Haik and Hajj 2016; Al-Haik et al. 2016) did not show a hysteresis with a window gap, it is concluded that the majority of the charge is being stored in the nanoparticles and not in the organic polymeric layer (Kim et al. 2012; Son et al. 2011; Shi et al. 2014).

3 Integrated Energy Harvesting/ Storage System

A Laird CP10,127,08 thermoelectric module was used as the energy harvester. This module contains 127 elements connected thermally in parallel and electrically in series. It has a square profile with a surface area of 30×30 mm^2 and a thickness of 4 mm. An electric hot plate, treated as the heat source, allowed the bottom side of the TEG to heat and provide sufficient temperature gradient. A solid aluminum plate with a copper pipe inserted through it is placed on the upper surface of the TEG and is used to recycle water from a large tank to maintain a constant cold temperature. Figure 2 depicts a schematic of the experimental setup. Two K-type thermocouples were used to measure temperatures on both sides of the TEG.

The TEG was connected in series with the organic storage device and four varying load resistors. A data acquisition card was used and recorded measurements of the voltage source, voltage across the organic capacitor and the temperature differences (ΔT). The voltage across the load is given by:

$$V_L = V_{TEG} - V_{cap} \tag{1}$$

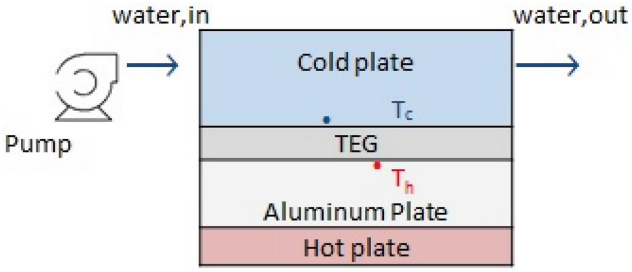

Figure 2: The experimental schematic for the TEG setup.

where V_{TEG} is the output voltage from the TEG and V_{cap} is the voltage measured across the organic capacitor. The current in a series connection can be calculated using:

$$I = \frac{V_L}{R_L} = \frac{V_{TEG} - V_{cap}}{R_L} \tag{2}$$

where R_L is load resistance.

4 Results and Discussion

The experiment consisted of two parts. For the first part, we raised the temperature of the hot plate for 20 minutes until reaching steady-state condition. The temperature difference is controlled by varying the temperature of the hot plate. For the second part, the TEG remains in steady-state condition for seven minutes after-which the TEG was cooled by turning off the heat source and recorded data for an additional 13 minutes. Four different load resistors, 100, 200, 330 and 460 Ω, were used in each experimental set. As the current begins to flow in the circuit, the generated charges are stored in the organic capacitor.

Figure 3 show the variation of the current and voltage across the capacitor versus time, when the heating source is turned on and off for the load resistance value of 100 Ω. For load resistors 220, 330, and 460 Ω, similar behaviors were observed however with different voltage and current values and are reported in Figures 4 and 5. We should note here that the experimental growth and decay associated with the charging and discharging of the TEG is not only associated with the time constant of the capacitor. As the temperature gradient increases, the time constant of the capacitor remains constant with the discharge rate. Rather, and because of the time variation of the heating source, the charging and discharging rates are associated with the heating and cooling rates of the hot plate. As such, we will consider here the impact of the load resistance and steady-state values of the hot temperature on the charging density of the capacitor. It was noticed that as

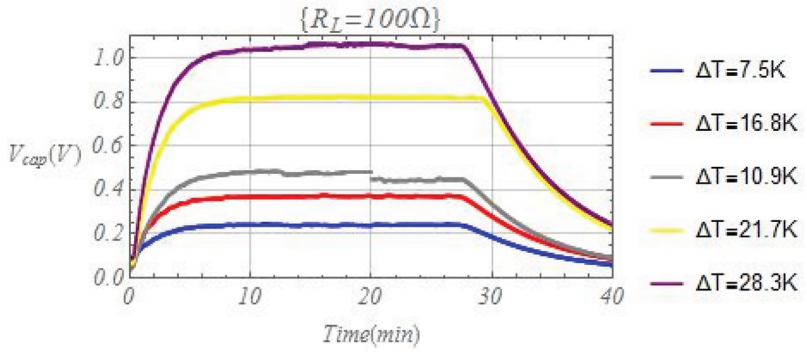

(a) The voltage across the organic capacitor versus time.

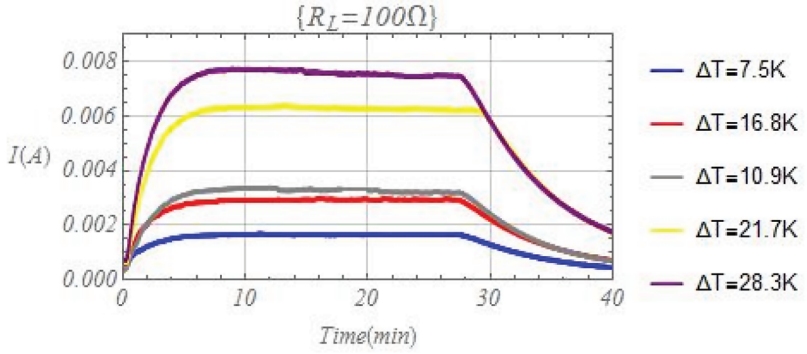

(b) The electrical circuit current versus time.

Figure 3: The experimental results with R_L = 100 Ω.

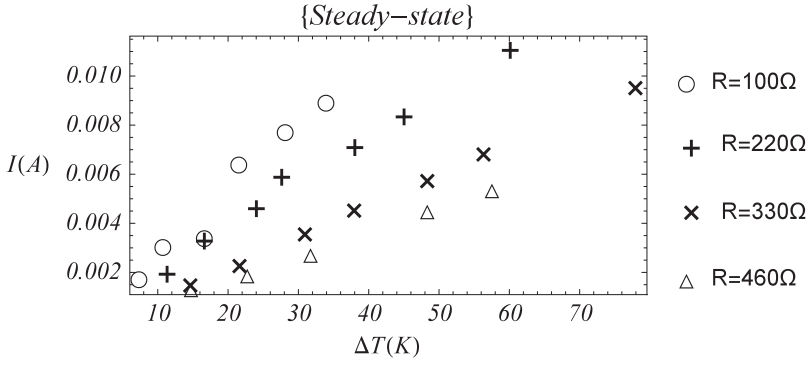

Figure 4: The average electrical circuit current versus temperature gradient at steady-state.

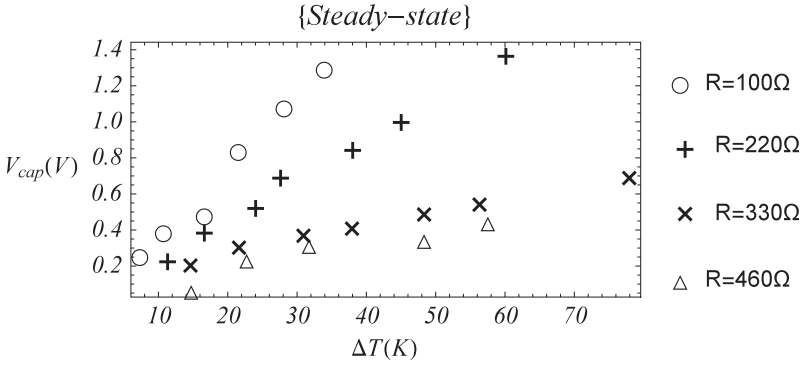

Figure 5: The average organic capacitor voltage versus temperature gradient at steady-state.

the load resistance is increased the temperature gradient also increased. For all load resistors, it took the capacitor 7 minutes to reach steady-state conditions, after-which it remains constant. The steady-state indicates that the maximum power is obtained for the certain temperature gradient. It is well known for TEG devices that the power output is proportional to the temperature difference (Montecucco, Siviter, and Knox 2014; Twaha et al. 2016).

For the 100 Ω, the minimum and maximum temperature gradient was reported to be 7.5 K and 28.3 K, respectively. Whereas, for the 460 Ω load resistor, the minimum and maximum temperature gradient was reported to be 14.7 K and 57.7 K, respectively. When placing the 220 Ω load resistor, the highest voltage and current values were obtained, 1.4 V and 0.011 A, respectively. We should note here that although the maximum values for voltage and current were obtained for 220 Ω load resistor, this does not imply that the maximum charge density is obtained for this load resistor. It was also observed that for the 330 and 460 Ω load resistors, the lowest voltage and current values were obtained although the maximum temperature gradient for the 330 Ω load resistor was obtained as 78.1 K.

Figure 4 shows the variation in the steady-state current as a function of the temperature difference, ΔT, for different load resistances. It is interesting to note that the steady-state current varies linearly with the temperature difference. The highest slope is for the load resistance of 100 Ω. This indicates that, at this load resistance, the capacitor can achieve a higher charge value at a specific value of temperature difference. This also can be seen in Figure 5, which shows the variations in the voltage across the capacitor as a function of temperature difference. For every value of temperature difference, the largest voltage is obtained for 100 Ω load resistance and decreases as the resistance is increased.

As shown in Figure 6, combining the results from the above figures shows that the internal resistance of the organic capacitor depends on the current. The low values of the load resistance lead to high values of the current which might have impacted the temperature of the capacitor itself and caused its resistance to increase significantly. So, in order for the capacitor to charge, the appropriate load resistance must be used. Values of voltage and current in Equations 1 and 2 have been averaged for steady-state condition.

The capacitance, C, of the capacitor was measured to be 100 nF using a multifunctional multimeter. The cross-sectional area of the capacitor, A_{cap}, is approximated to be 0.25 cm^2. Therefore, the average charge density can be expressed as:

$$\dot{q}_{charge} = \frac{CV_{cap}}{A_{cap}} \tag{3}$$

Figure 7 shows that the charge density is a function of the temperature difference and the load resistance. For a specific value of temperature difference, the highest charge density is obtained when the load resistance is 100 Ω. Particularly, a maximum charge density of $5.14 \times 10^{-3} \frac{C}{m^2}$ is obtained for temperature difference of 34.1 K. Table 1 shows the reduction in charge density as the load resistance is increased.

For a load resistance below 100 Ω, very low to no current was detect. Electrical current was detected for resistance values that were larger than 100 Ω. At higher resistances the steady-state current decreased as the load resistance increased. Therefore, we only tested it up to 460 Ω. The internal resistance of the capacitor was determined by a simulated system and was found to be about 100 Ω. The matching of resistive load and the capacitor seems to provide the optimal configuration for the current and voltage at lower temperature gradients. Higher temperature gradient was required to produce the measurable current for higher load resistors to pass through the system.

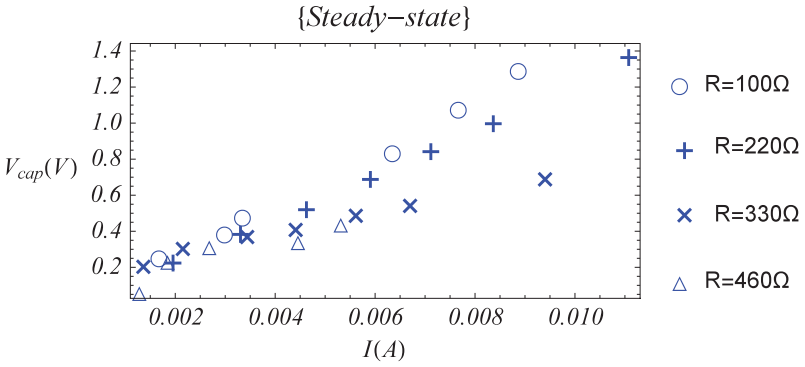

Figure 6: The average voltage across the organic capacitor versus average circuit current.

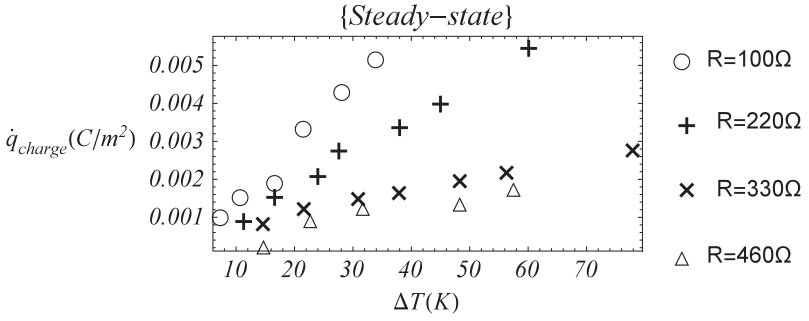

Figure 7: The average charge density versus temperature gradient.

Table 1: The charge density reduction percentage with respect to load resistance.

R_L (Ω)	$\frac{d\dot{q}_{charge}}{d(\Delta T)}$ (10^{-5})	Reduction (%)
100	15	–
220	9	40
330	4	73.3
460	3	80

5 Conclusions

We investigated the integration of a TEG module with an organic capacitor. The effect of the load resistance and steady-state values of the TEG's temperature difference on the charging density of the organic capacitor were investigated. The charging and discharging of the TEG are not associated with the time constant of the capacitor. The current flowing through the circuit board and the temperature difference have a linear relationship. The slope value of both the voltage and current increases as the load resistance decreased. Also, a linear relation was noticed between the temperature difference and the voltage across the capacitor. The highest voltage values across the capacitor for all temperature differences occur when the load resistance is 100 Ω. The organic capacitor's internal resistance depends on the current of the circuit. The current value increased as the load resistance was decreased. The high values of electrical current could increase the temperature of the capacitor, which increases the internal resistance of the capacitor. Therefore, a suitable load resistance should be used with the capacitor to be able to charge. For all temperature differences, the charging density of the capacitor rates were the highest at the 100 Ω load resistance. The reduction in charge density rates based on the highest values are 40 %, 73 % and 80 % for load resistances of 220 Ω, 330 Ω and 460 Ω, respectively.

Acknowledgment: This research did not receive any specific grant from funding agencies in the public, commercial, or not-for-profit sectors.

References

Ismail B. I., and W. H. Ahmed. 2009. "Thermoelectric Power Generation using Waste-heat Energy as an Alternative Green Technology." *Recent Patents on Electrical Engineering* 2 (1): 27–39.

Kristiansen N., G. Snyder, H. Nielsen, and L. Rosendahl. 2012. "Waste Heat Recovery from a Marine Waste Incinerator using a Thermoelectric Generator." *Journal of Electronic Materials* 41 (6): 1024–1029.

Samson D., M. Kluge, T. Fuss, U. Schmid, and T. Becker. 2012. "Flight Test Results of a Thermoelectric Energy Harvester for Aircraft." *Journal of Electronic Materials* 41 (6): 1134–1137.

Hsiao Y., W. Chang, and S. Chen. 2010. "A Mathematic Model of Thermoelectric Module with Applications on Waste Heat Recovery from Automobile Engine." *Energy* 35 (3): 1447–1454.

Hsu C.-T., G.-Y. Huang, H.-S. Chu, B. Yu, and D.-J. Yao. 2011. "Experiments and Simulations on Low-temperature Waste Heat Harvesting System by Thermoelectric Power Generators." *Applied Energy* 88 (4): 1291–1297.

Sargentis C., K. Giannakopoulos, A. Travlos, and D. Tsamakis. 2007. "Fabrication and Electrical Characterization of a MOS Memory Device Containing Self-assembled Metallic Nanoparticles." *Physica E: Low-dimensional Systems and Nanostructures* 38 (1–2): 85–88. Proceedings of the E-MRS 2006 Symposium C: Silicon Nanocrystals for Electronic and Sensing Applications.

Mabrook M., Y. Yun, C. Pearson, D. Zeze, and M. Petty. 2009. "A Pentacene-based Organic Thin Film Memory Transistor." *Applied Physics Letters* 94 (April): 173302.

Mabrook M. F., C. Pearson, D. Kolb, D. A. Zeze, and M. C. Petty. 2008. "Memory Effects in Hybrid Silicon-Metallic Nanoparticle-organic thin Film Structures." *Organic Electronics* 9 (5): 816–820.

Guan W., S. Long, M. Liu, Z. Li, Y. Hu, and Q. Liu. 2007. "Fabrication and Charging Characteristics of MOS Capacitor Structure with

Metal Nanocrystals Embedded in Gate Oxide." *Journal of Physics D: Applied Physics* 40 (9): 2754.

Gupta R. K., D. Y. Kusuma, P. Lee, and M. Srinivasan. 2012. "Copper Nanoparticles Embedded in a Polyimide film for Non-volatile Memory Applications." *Materials Letters* 68 (0): 287–289.

Sleiman A., M. Rosamond, M. A. Martin, A. Ayesh, A. A. Ghaferi, A. Gallant, M. Mabrook, and D. Zeze. 2012. "Pentacene-based Metal-Insulator-Semiconductor Memory Structures Utilizing Single Walled Carbon Nanotubes as a Nanofloating Gate." *Applied physics letters* 100 (January): 023302.

Duguay S., S. Burignat, P. Kern, J. J. Grob, A. Souifi, and A. Slaoui. 2007. "Retention in Metal-Oxide-Semiconductor Structures with Two Embedded Self-aligned Ge-Nanocrystal Layers." *Semiconductor Science and Technology* 22 (8): 837.

Haik M. Y., A. I. Ayesh, T. Abdulrehman, and Y. Haik. 2014. "Novel Organic Memory Devices Using au-pt-ag Nanoparticles as Charge Storage Elements." *Materials Letters* 124 (0): 67–72.

Al-Haik M. Y., Y. Haik, and M. R. Hajj. 2017. "Characterization of CdS and AgPt Nanofillers used in Organic Capacitors." *Synthetic Metals* 223: 26–33.

Al-Haik M. Y., and M. R. Hajj. 2016. "Integrated Piezoelectric Energy Harvesting and Organic Storage System." *Energy Harvesting and Systems* 3 (2): 113–119.

Al-Haik M. Y., M. Y. Zakaria, M. R. Hajj, and Y. Haik. 2016 "Storage of Energy Harvested from a Miniature Turbine in a Novel Organic Capacitor." *Journal of Energy Storage* 6: 232–238.

Kim Y.-H., M. Kim, S. Oh, H. Jung, Y. Kim, T.-S. Yoon, Y.-S. Kim, and H. Ho Lee. 2012. "Organic Memory Device with Polyaniline Nanoparticles Embedded as Charging Elements." *Applied Physics Letters* 100 (16): 91.

Son D. I., D. H. Park, J. B. Kim, J.-W. Choi, T. W. Kim, B. Angadi, Y. Yi, and W. K. Choi. 2011. "Bistable Organic Memory Device with Gold Nanoparticles Embedded in a Conducting Poly(n-vinylcarbazole) Colloids Hybrid." *The Journal of Physical Chemistry C* 115 (5): 2341–2348.

Shi Q., J. Xu, Y. Wu, Y. Wang, X. Wang, Y. Hong, L. Jiang, and L. Li. 2014. "Electrical Bistable Properties of Hybrid Device Based on sio2 Modified-zno Nanoparticles Embedded in Poly-4-vinyl-phenol." *Physics Letters A* 378 (47): 3544–3548.

Montecucco A., J. Siviter, and A. R. Knox. 2014. "The Effect of Temperature Mismatch on Thermoelectric Generators Electrically Connected in Series and Parallel." *Applied Energy* 123: 47–54.

Twaha S., J. Zhu, Y. Yan, and B. Li. 2016 "A Comprehensive Review of Thermoelectric Technology: Materials, Applications, Modelling and Performance Improvement." *Renewable and Sustainable Energy Reviews* 65: 698–726.